Drug Design, Development and Therapy

ISSN: (Print) (Online) Journal homepage: www.tandfonline.com/journals/dddt20

Buyang Huanwu Decoction Alleviates Ischemic Stroke Injury by Inhibiting Ferroptosis via the Nrf2/GPX4 Pathway

Hao Huang, Sijie Liu, Jing Wu, Jiayi Zhu, Jiaxiang Xu, Shuhong Yu, Lingna Bei, Biao Zhang & Yi Luo

To cite this article: Hao Huang, Sijie Liu, Jing Wu, Jiayi Zhu, Jiaxiang Xu, Shuhong Yu, Lingna Bei, Biao Zhang & Yi Luo (2025) Buyang Huanwu Decoction Alleviates Ischemic Stroke Injury by Inhibiting Ferroptosis via the Nrf2/GPX4 Pathway, Drug Design, Development and Therapy, , 2285-2305, DOI: 10.2147/DDDT.S503424

To link to this article: https://doi.org/10.2147/DDDT.S503424

Published online: 27 Mar 2025.

Drug Design, Development and Therapy

Dovepress
Taylor & Francis Group

Open Access Full Text Article

ORIGINAL RESEARCH

Buyang Huanwu Decoction Alleviates Ischemic Stroke Injury by Inhibiting Ferroptosis via the Nrf2/GPX4 Pathway

Hao Huang[1,*], Sijie Liu[1,*], Jing Wu[2,*], Jiayi Zhu[1], Jiaxiang Xu[1], Shuhong Yu[1], Lingna Bei[1], Biao Zhang[1,3], Yi Luo[1]

[1]Department of Neurology, Suzhou Hospital of Integrated Traditional Chinese and Western Medicine, Suzhou, People's Republic of China; [2]Department of Traditional Chinese Medicine, Community Health Service Center of the Urban Area, Suzhou, People's Republic of China; [3]Central laboratory, Suzhou Hospital of Integrated Traditional Chinese and Western Medicine, Suzhou, People's Republic of China

*These authors contributed equally to this work

Correspondence: Yi Luo; Biao Zhang, Suzhou Hospital of Integrated Traditional Chinese and Western Medicine, No. 39, Xiashatang, Mudu Town, Wuzhong District, Suzhou City, 215101, People's Republic of China, Email yiluomdyy@126.com; zhangbmed@126.com

Purpose: Acute ischemic stroke poses major challenges due to high disability and mortality rates. Ferroptosis, a form of regulated cell death triggered by iron-induced oxidative stress, plays a key role in stroke injury. Despite its long history in stroke treatment, the mechanism of Buyang Huanwu Decoction (BHD) in ferroptosis remains unclear.

Methods: Network pharmacology predicted BHD's active components and pathways, while Ultra Performance Liquid Chromatography-Tandem Mass Spectrometry (UPLC-MS/MS) confirmed its main ingredients. Middle Cerebral Artery Occlusion (MCAO) was induced in C57 mice, with neurological deficits and infarct size assessed by Longa scoring and TTC staining. Histopathological and ultrastructural changes were assessed by staining and electron microscopy, and biochemical markers (MDA, GSH, SOD, Fe^{2+}) measured by kits. Western blotting and qPCR analyzed ferroptosis-related proteins, Nrf2 localization, and gene expression. In vitro, HT22 cells viability and ROS levels were assessed under Oxygen-Glucose Deprivation/Reoxygenation (OGD/R) conditions. Protein expression, Nrf2 interactions, and nuclear translocation were also investigated.

Results: Network pharmacology showed BHD targets key pathways in cerebral infarction, including ferroptosis and antioxidant pathways. BHD improved neurological function and reduced the infarct size in MCAO mice by 10% - 50%, and also significantly decreased the levels of oxidative stress markers (MDA, Fe^{2+}) while increasing the activities of antioxidants (GSH, SOD). Histopathological and ultrastructural analyses demonstrated reduced neuronal damage and improved mitochondrial structure. Western blot and qPCR indicated upregulation of GPX4 and Nrf2, downregulation of Keap1, and Nrf2 nuclear translocation. In vitro, BHD enhanced HT22 cell viability and reduced ROS under stress. Protein analysis confirmed increased Nrf2, GPX4, and HO-1, with decreased Keap1 and enhanced Nrf2 nuclear translocation. Nrf2 inhibitor experiments confirmed BHD's effects are Nrf2-mediated.

Conclusion: In pre-clinical studies, BHD exerts neuroprotective effects in ischemic stroke by inhibiting ferroptosis through the Nrf2/GPX4 pathway.

Keywords: ischemic stroke, ferroptosis, Nrf2/GPX4 pathway, buyang huanwu decoction

Introduction

Ischemic stroke has become a major public health concern, with increasing incidence and mortality rates in recent years.[1] Many survivors experience lasting functional impairments, resulting in significant health challenges and socioeconomic burdens. Early reperfusion through intravenous thrombolysis or mechanical thrombectomy is crucial for salvaging the ischemic penumbra in ischemic stroke treatment.[2] However, ischemia-reperfusion injury still leads to neuronal death and lasting functional deficits, remaining a major cause of poor outcomes in ischemic stroke.[3] Preventing or minimizing

Received: 26 November 2024
Accepted: 20 March 2025
Published: 27 March 2025

Graphical Abstract

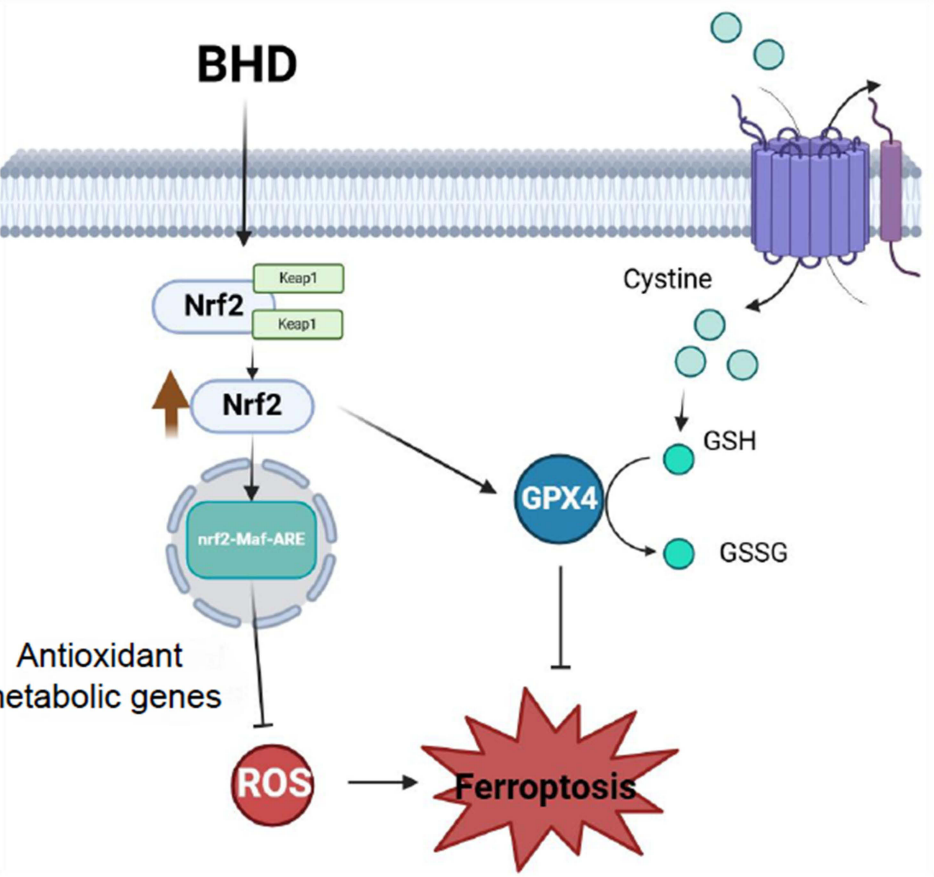

neuronal death after a stroke is crucial for advancing treatment outcomes. In ischemic stroke, iron accumulation and redistribution, glutamate buildup, oxidative stress, lipid peroxidation, and epigenetic regulation are key drivers of ferroptosis, positioning it as a central mechanism in stroke pathology and neuronal death.[4] Studies show that ferroptosis inhibitors can protect neurons from ischemia-reperfusion damage, strongly suggesting that inhibiting neuronal ferroptosis is a critical therapeutic target for treating ischemic stroke and reperfusion injury.[5]

Ferroptosis, a form of regulated cell death characterized by iron - dependent lipid peroxidation, is closely linked to the severity of ischemia - reperfusion injury in the brain.[6] The Nrf2/GPX4 pathway plays a pivotal role in protecting against oxidative stress. Numerous studies have shown that Nrf2 is crucial in regulating iron, lipid, and amino acid metabolism, and Nrf2 knockout animals are more susceptible to ischemic stroke, highlighting the critical role of this transcription factor in protecting neurons from ferroptosis during ischemic stroke.[7,8] Neurons in the brain are rich in polyunsaturated fatty acids, which act as substrates for lipid peroxidation, making them more vulnerable to Lipid Peroxidation (LPO) during ischemia.[9] The rapid depletion of ATP during ischemia leads to uncontrolled ion leakage across cell membranes, causing membrane depolarization and glutamate release, which activates phospholipases and triggers the release of arachidonic acid/adenosine deaminase (AA/ADA), ultimately contributing to the formation of ferroptosis substrates.[10] Simultaneously, regulators of iron homeostasis, including iron transport proteins, undergo changes that lead to iron accumulation. Neurons readily absorb this unbound iron, leading to intracellular iron overload, oxidative stress, and ultimately, neuronal death.[11] Previous studies have confirmed that iron chelators can reduce neuronal damage after ischemic events in animals,[12] while ferroptosis inhibitors can rescue neurons from ischemic stroke-induced death.[13]

However, due to issues regarding efficacy and safety, the direct clinical application of ferroptosis inhibitors remains challenging to achieve.

Buyang Huanwu Decoction (BHD), a traditional Chinese medicine (TCM) formula from Wang Qingren's *Yi Lin Gai Cuo*, is commonly used to promote neurological recovery in stroke and paralysis patients.[14] In TCM, ischemic stroke is mainly attributed to Qi deficiency, with phlegm and blood stasis as secondary factors. Treatment mainly focuses on replenishing Qi and resolving blood stasis. BHD is composed of

> Huangqi (Radix Astragali) 60g, Danggui Wei (Radix Angelicae Sinensis) 6g, Chishao (Radix Paeoniae Rubra) 4.5g, Dilong (Pheretima) 3g, Chuanxiong (Rhizoma Chuanxiong) 3g, Taoren (Semen Persicae) 3g, and Honghua (Flos Carthami) 3g.

The formula emphasizes Huangqi, which significantly tonifies Qi and promotes blood circulation as the primary herb. Clinically, BHD is commonly used to treat syndromes of Qi deficiency and blood stasis obstructing the meridians, which aligns with the etiology and pathogenesis of ischemic stroke. Modern research has demonstrated that BHD significantly improves neurological deficits in ischemic stroke patients and exhibits neuroprotective effects in various animal models of the condition.[15] BHD contains multiple antioxidant compounds that effectively scavenge free radicals, reduce oxidative stress, and elevate superoxide dismutase levels in brain tissue.[16] Among them, Radix Astragali is used in the largest amount. Astragalus polysaccharide has been proven to significantly reduce malondialdehyde (MDA) and increase superoxide dismutase (SOD) levels.[17] However, due to the complexity of the multi - target effects of traditional Chinese medicine compounds, exploring the mechanism of BHD in treating ischemic stroke becomes more variable. Currently, there is no research indicating that BHD can play a neuroprotective role in cerebral infarction by activating the Nrf2/GPX4 pathway to inhibit neuronal ferroptosis. Therefore, we intend to use network pharmacology methods to explore the therapeutic role of BHD in the treatment of ischemic stroke and its underlying mechanisms, focusing on its effects on Nrf2 activation and GPX4/GSH pathway regulation in preventing neuronal ferroptosis. The findings of this research are expected to contribute to developing alternative stroke therapies, providing new insights and potential strategies for the treatment of this prevalent and devastating disease.

However, the pathophysiology of ischemic stroke in humans is highly complex, influenced by factors such as age, sex, comorbidities, and genetic background. As a preclinical study, our research provides mechanistic insights into the potential neuroprotective effects of BHD, but further clinical validation is necessary to confirm its therapeutic applicability in diverse patient populations.

Material and Methods

Construction and Analysis of Network Pharmacology

Active Ingredient Screening and Target Prediction of BHD

In the Traditional Chinese Medicine System Pharmacology Database and Analysis Platform (TCMSP, http://lsp.nwu.edu.cn/tcmsp.php), we screened for the active ingredients of BHD based on the criteria of oral bioavailability (OB) ≥ 30% and drug likeness (DL) ≥ 0.18, identifying Astragalus, Angelica, Red Peony, Chuanxiong, Peach Kernel, Safflower, and Earthworm as effective components. We obtained the SMILES numbers and Mol2 structures of all compounds from the PubChem (https://pubchem.ncbi.nlm.nih.gov/) and TCMSP databases. Subsequently, we identified the corresponding targets for these compounds using the SwissTargetPrediction (http://swisstargetprediction.ch/) and PharmMapper (https://www.lilab-ecust.cn/pharmFigureper/) databases.

Acquisition of Disease-Related Target Gene Database

We searched for disease targets in the GeneCards (https://www.genecards.org/), OMIM (https://www.omim.org/), and TTD (https://db.idrblab.net/ttd/) databases. All target genes were normalized and imported into the UniProt database (https://www.uniprot.org/) to obtain UniProt IDs and removing duplicates.

Acquisition of Compound-Disease Common Targets and PPI Networks

We calculated the common targets of drugs and diseases using Venny 2.1 (https://bioinfogp.cnb.csic.es/tools/venny/index.html) and obtained a Venn diagram. Using the STRING database (https://string-db.org/), we input the intersection

of drug targets and disease targets, set the species to "Homo sapiens", and imported the resulting data file into Cytoscape for visualization.

GO and KEGG Network Analysis

We imported the intersecting genes of drugs and diseases into the DAVID database (https://david.ncifcrf.gov/) to perform Gene Ontology (GO) analysis for cellular components (CC), molecular functions (MF), and biological processes (BP). We then obtained pathway-related data for KEGG analysis. The top 10 GO terms with the smallest *P*-values and the top 20 KEGG pathways were imported into a bioinformatics mapping website (http://www.bioinformatics.com.cn/) to create bar plots and bubble plots. Finally, we imported the 20 core pathways and their corresponding target proteins into Cytoscape to construct a "key pathway-target" network for HBD intervention in patients with cerebral infarction.

Experimental Validation

Preparation of Buyang Huanwu Decoction and Medicated Serum

BHD comprised of 60g Astragalus, 10g Paeonia lactiflora, 10g Angelica sinensis, 10g Ligusticum, 10g Lumbricus, 10g Prunus persica, and 10g Carthamus tinctorius. Mix all herbal ingredients with 500 mL of water and boil. Repeat the boiling process twice, each time for 1 hour. Concentration and sterilization: After boiling, filter and mix the mixture. Concentrate the mixture to approximately 90 mL using a rotary evaporator under vacuum. The resulting liquid is dark brown, with 1 mL equivalent to 1.3 grams of raw material. After high-temperature, high-pressure steam sterilization, store the decoction in sterile sealed infusion bottles for subsequent experiments.Preparation of medicated serum: According to the dosage required for the high-dose group of mice (15.6 g/kg body weight). Administer BHD by gastric lavage, twice daily for 7 days. At the end of the treatment period, collect blood samples from anesthetized mice at the apex of the heart. Centrifuge the samples at 3000 rpm for 10 minutes. Collect the supernatant after centrifugation and store it at −80°C for subsequent experimental analysis (Figure 1A and B).

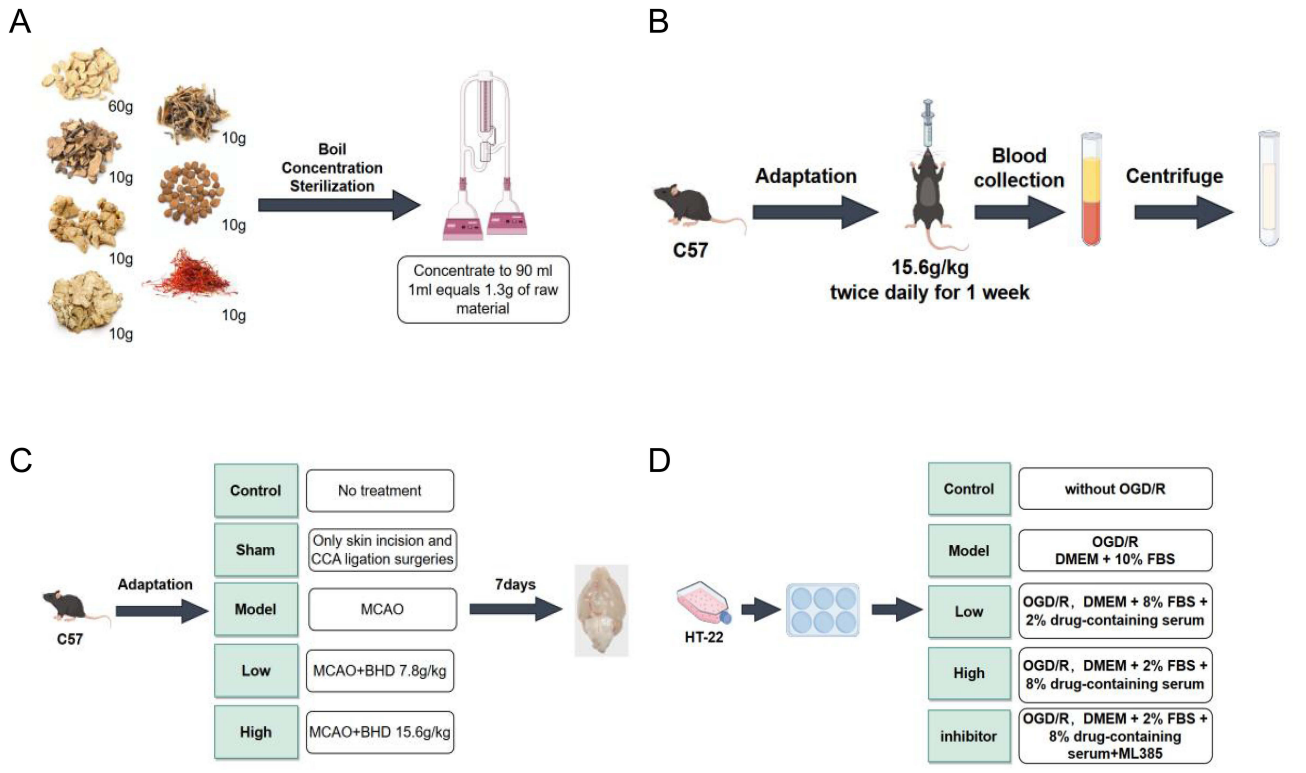

Figure 1 (**A**) Preparation of BHD. (**B**) Preparation of medicated serum. (**C**) Animal experiments and treatment. (**D**) The experimental design of Cells.

Liquid Chromatography - Tandem Mass Spectrometry

The UPLC-MS/MS analysis was performed using a Shimadzu LCMS-8050 ultra-high-performance liquid chromatography-tandem mass spectrometry (UHPLC-MS/MS) system (Shimadzu, Japan) to quantify six major components in Buyang Huanwu Decoction (BHD). All reference standards were purchased from the National Institutes for Food and Drug Control (China) and diluted to appropriate concentrations as standard solutions. For sample preparation, 10 mL of BHD extract (crude drug concentration: 1 g/mL) was precisely measured and diluted to 50 mL with 50% acetonitrile aqueous solution. The mixture was vortexed for 30s, followed by centrifugation at 8000 r/min for 5 min. Subsequently, 1 mL of the supernatant was further diluted to 50 mL with 50% acetonitrile aqueous solution, vortexed for 30s, and filtered through a 0.22 μm microporous membrane. The resulting filtrate was used as the sample solution for multiple reaction monitoring (MRM) analysis. Chromatographic separation was conducted using an ACQUITY UPLC® HSS T3 column (2.1 mm × 100 mm, 1.8 μm). The mobile phase consisted of 0.1% formic acid in water (A) and acetonitrile (B), employing a gradient elution mode. An electrospray ionization (ESI) source was utilized in both positive and negative ion modes, with optimized ion pairs for each compound. The MRM mode was used for quantitative analysis of the target components.

Animal Experiments and Treatment

The mice are all male C57 mice, aged 6 to 8 weeks, purchased from Nanjing Qinglongshan Biotechnology, production license number: SCXK(Su)2024–001. All animal procedures were conducted following the Guidelines for the Ethical Review of Laboratory Animal Welfare (China, 2018) and approved by the Experimental Animal Ethics Committee of Suzhou Hospital of Integrated Traditional Chinese and Western Medicine (Ethics No. 2023009). This study consisted of 5 groups of 6 mice each, and all experiments were repeated three times independently. All mice were randomly divided into groups by means of the random number table method, and all operators were blinded. Control group (Control): These animals receive no treatment or intervention and serve as the comparative baseline. Sham surgery group (Sham): Only undergo skin incision and common carotid artery ligation surgeries without middle cerebral artery occlusion (MCAO) implantation. This group simulates the effects of surgery on animals.Model group (Model): MCAO surgery is performed using the filament method to establish an ischemic stroke model.High-dose BHD group (High): In addition to MCAO surgery, mice receive high-dose (15.6 g/kg body weight) BHD treatment administered orally twice daily for one week. Low-dose BHD group (Low): Similar to the high-dose group, these animals also undergo MCAO surgery and receive low-dose (7.8 g/kg body weight) BHD treatment administered orally twice daily for one week (Figure 1C).

Establishment of Animal Models of Ischemic Stroke

Before surgery, mice are fasted for 12 hours and deprived of water. They are anesthetized by inhalation anesthesia (RWD R510-22-10) prior to surgery and prepared and disinfected. Throughout the entire surgical procedure, mice are placed on a heating pad to maintain their body temperature. Firstly, the common carotid artery is isolated and separated. Then, a small incision is made on the common carotid artery using small scissors to prepare for fiber insertion. The prepared fiber (RWD MSMC19B100PK50) is inserted through the incision in the common carotid artery. The fiber is advanced forward until resistance is felt, indicating it has reached the predetermined mark, successfully occluding the middle cerebral artery, resulting in focal ischemia. After successful establishment of the MCAO model, the proximal common carotid artery is ligated.[18,19] After surgery, place the mice in a warm and quiet environment, closely monitor their vital signs, provide easily digestible food and water, regularly check the surgical wounds, and assess neurological function.

Neurological Function Score

Using the Longa neurological deficit scoring system, a 5-point scale for assessing neurological deficits is employed. A score of 0 indicates no neurological deficit. A score of 1 indicates mild focal neurological deficit, manifested by incomplete extension of the left forepaw. A score of 2 indicates moderate focal neurological deficit, manifested by circling to the left. A score of 3 indicates severe focal functional impairment, with the mouse falling to the left. A score of 4 indicates the mouse's inability to walk spontaneously, exhibiting a decreased level of consciousness.[18]

TTC Staining

24 hours post-induction of cerebral ischemia, mice are re-anesthetized, euthanized, and their brain tissues are extracted. The brains are then rinsed in 4°C PBS for 5 minutes. Sectioning and Staining: Coronal sections of the brain are made at 2mm intervals, producing 5 slices. These sections are then immersed in a freshly prepared 1% TTC solution for a water bath at 37°C for 10 minutes. After staining, the slices are rinsed with saline and fixed in 10% formaldehyde for color photography.

HE Staining

Perfuse mouse brain with pre-cooled PBS until the brain color lightens. Then, remove the brain tissue and fix it in 4% paraformaldehyde. After dehydration, embed the tissue in paraffin and section. Then, stain these sections with hematoxylin and eosin. Following HE staining, observe pathological changes in brain tissue under a microscope.

Nissl Staining

Perfuse mouse brain with pre-cooled PBS until the brain tissue color becomes lighter. Following perfusion, carefully extract and fix brain tissue in 4% paraformaldehyde. After dehydration of brain tissue, embed in paraffin and section. Mount sections on slides and perform Nissl staining using cresyl violet. After staining, rinse sections with alcohol and dehydrate, then cover. Subsequently, observe stained sections under a light microscope.

Transmission Electron Microscopy (TEM)

Prepare tissue section copper grids for experiments involving the collection of brain tissues from different groups of mice, embedding, ultrathin sectioning, lead uranium double staining, negative staining, etc. Perform transmission electron microscopy imaging (Hitachi HT7800 transmission electron microscope) using the Hitachi TEM system.

Biochemical Assay

Refer to the instruction manual provided by the reagent manufacturer and follow the operational procedures accordingly. Lipid Peroxidation MDA Assay Kit (Beyotime, S0131S), Ferrous Ion Content Assay Kit (Biosharp,BL1147B), GSH Assay Kit (Nanjing Jiancheng Technology, A006-2-1). SOD Assay Kit (Nanjing Jiancheng Technology, A001-3-2).

Cell Experimental Setup and Model Establishment

HT22 cells, purchased from icell in Shanghai, China. Cells within passages 3–10 were utilized for all experiments to ensure consistency and viability. To create an oxygen-glucose deprivation/reperfusion (OGD/R) model, cells were plated in 6-well plates until 80% confluence. For OGD, glucose- and serum-free DMEM was used in a hypoxic chamber (1% O2, 5% CO2, 94% N2). Cells underwent OGD for various durations (0.5–3 hours) to find the best hypoxia time. After OGD, cells were returned to normal conditions with DMEM and 10% FBS for 24 hours. CCK-8 assays determined that 2 hours of OGD followed by 24 hours of reperfusion was best. Cells were divided into five groups. Each group contained 6 independent samples and the experiment was repeated 3 times: control (standard conditions), model (OGD/R under standard conditions), low-dose (OGD/R with 8% FBS and 2% drug-containing serum), high-dose (OGD/R with 2% FBS and 8% drug-containing serum), and inhibitor group (OGD/R with 2% FBS, 8% drug-containing serum, and ML385 inhibitor) (Figure 1D).

Cell Viability Assay (CCK-8)

Following the CCK-8 reagent instructions (Medicalbio, CCK04), cells in different groups were processed. Subsequently, absorbance at 450 nm was measured using a microplate reader.

Real-Time Quantitative PCR

Mouse brain tissue was collected and total RNA was extracted using the Tissue Mag-Beads RNA Extraction Kit (Medicalbio, MR0112). The extracted RNA was reverse transcribed into cDNA using the reverse transcription kit (Vazyme, R423-01). Real-time quantitative PCR (qPCR) was performed using the SYBR Green PCR Master Mix

Table 1 Primer Sequences for qRT-PCR

Gene	Forward Primer (5'-3')	Reverse Primers (5'-3')
Nrf2	AGTTGTAGCCTCGGGAAGTTGTTAG	AGCCTCTTGGTTTCTGTCACTCATC
HO-1	AAGACCGCCTTCCTGCTCAAC	TCTGACGAAGTGACGCCATCTG
FSP1	CCACAGCACGAGACCAAGGAG	GTGAGTGTTGTTAGGAGGGAAGGAG
ASCL3	TCTGTTTCTGCTGTCCCGTTGG	AAATAGCCACCTTCCTCCCAGTTC
ASCL4	TTAGAACGCTGGTGGAATCCTACG	ATCAATCAGCAACAGCAAGCAGAC
P53	CGCCGACCTATCCTTACCATCATC	CTCCCAGGGCAGGCACAAAC
SLA3A2	CTGCGGCTAGGCGGTTCTTAC	CGTCGGTGGAGTGTTCAGTAGG
SLA7A11	TGGTCTTGTCACTTGGCATCTGG	TCTCTCACCCTCACCCTCTAAGC
β-actin	GTGCTATGTTGCTCTAGACTTCG	ATGCCACAGGATTCCATACC

(Vazyme, Q712) according to the manufacturer's instructions.The primer amplification was determined to be a single peak through the melting curve, and the efficiency of the primer pairs was confirmed to be within the range of 90% to 110% through the efficiency test. The relative mRNA expression levels were calculated based on the obtained CT values (Table 1).

Western Blotting Analysis

Brain tissue was homogenized in RIPA lysis buffer, lysed on ice for 30 minutes, sonicated, and centrifuged at 12,000 rpm for 15 minutes at 4°C. The supernatant was collected for BCA protein quantification. Nuclear proteins were extracted using a nuclear extraction kit according to the manufacturers' instructions. Samples were mixed with loading buffer, heated at 95°C for 10 minutes, and loaded onto an SDS-PAGE gel. A prestained molecular weight protein marker (10–180 kDa, Biodragon) was used as the marker. After electrophoresis, proteins were transferred to methanol-activated PVDF membranes and blocked with 5% skim milk for 1 hour at room temperature. The membranes were incubated overnight at 4°C with primary antibodies: β-actin (Biodragon, B0099, 1:7500), Nrf2 (ZEN-BIOSCIENCE, 380773, 1:1000), Heme Oxygenase 1 (ZEN-BIOSCIENCE, 380753, 1:1000), Keap1 (Biodragon, R26935, 1:1000), and Glutathione Peroxidase 4 (ZEN-BIOSCIENCE, 381958, 1:1000). Lamin B (ZEN-BIOSCIENCE, RM0733, 1:1000) was used as a nuclear loading control. After washing with PBST, membranes were incubated with HRP-conjugated secondary antibody (HRP-Goat anti-rabbit IgG (H+L), Biodragon, BF03008, 1:10000) for 45 minutes at room temperature, then developed using ECL detection (Medicalbio, PT01001).

Immunoprecipitation (IP)

Brain tissue lysates were incubated with Nrf2 antibody (ZEN-BIOSCIENCE, 380773) overnight at 4°C, followed by incubation with Protein A/G magnetic beads for 2 hours. Immune complexes were washed, eluted, and analyzed by SDS-PAGE and Western blotting. Ubiquitin (Biodragon, RM4934, 1:1000) was detected to assess Nrf2 ubiquitination, and membranes were re-probed with Nrf2 antibody to confirm equal loading.

Flow Cytometry

Flow cytometry was performed to assess reactive oxygen species (ROS) levels. Cells were incubated with ROS (Yeasen Biotechnology, 50101ES01) following the manufacturer's instruction and analyzed using a flow cytometer (Beckman, DxFlex). Data were processed with FlowJo software.

Immunofluorescence

For immunofluorescence analysis of Nrf2, HT22 cells were fixed with 4% paraformaldehyde for 15 minutes at room temperature. The cells were then permeabilized with 0.1% Triton X-100 for 10 minutes and blocked with 5% BSA for 1 hour to prevent nonspecific binding. Subsequently, the cells were incubated overnight at 4°C with a primary Nrf2 antibody (ZEN-BIOSCIENCE, 380773, 1:100). After washing, the cells were incubated with a Multi-rAb CoraLite® Plus 488-Goat Anti-Rabbit Recombinant Secondary Antibody (H+L)(Proteintech, RGAR002, 1:500) for 1 hour at room temperature. The nuclei

were counterstained with DAPI (Beyotime, C1006) for 5 minutes. Finally, the cells were imaged using a fluorescence microscope (Olympus, IX73), and the images were analyzed using Image J software to quantify Nrf2 nuclear translocation.

Statistical Analyses

All data are presented as mean±standard deviation (Mean±SD), and statistical analysis was performed using Prism GraphPad 9.0 software. Each experiment was independently repeated at least three times to ensure reliability. All the data follow a normal distribution. Between-group comparisons were conducted using a two-tailed *t*-test for two-group comparisons. The assumption of normal distribution and homogeneity of variance was verified for all datasets; if these assumptions were not met, non-parametric tests were applied. A p-value of <0.05 was considered statistically significant.

Results

Common Targets of BHD and Cerebral Infarction Analysis

In the TCMSP database, a total of 102 effective active compounds of BHD were identified based on oral bioavailability (OB) and drug-likeness (DL). This included 20 compounds from Astragalus, 2 from Angelica, 28 from Radix Paeoniae Rubra, 7 from Chuanxiong, 23 from Persica, 22 from Carthamus, and 0 from Earthworm. The typical SMILES of these 102 compounds were retrieved from the PubChem database and imported into Swiss Target Prediction and PharmMapper. After excluding targets with a confidence level of 0 and duplicates, a total of 924 potential targets for the effective components of BHD were obtained (Figure 2). By searching "cerebral infarction" in the GeneCards, OMIM,

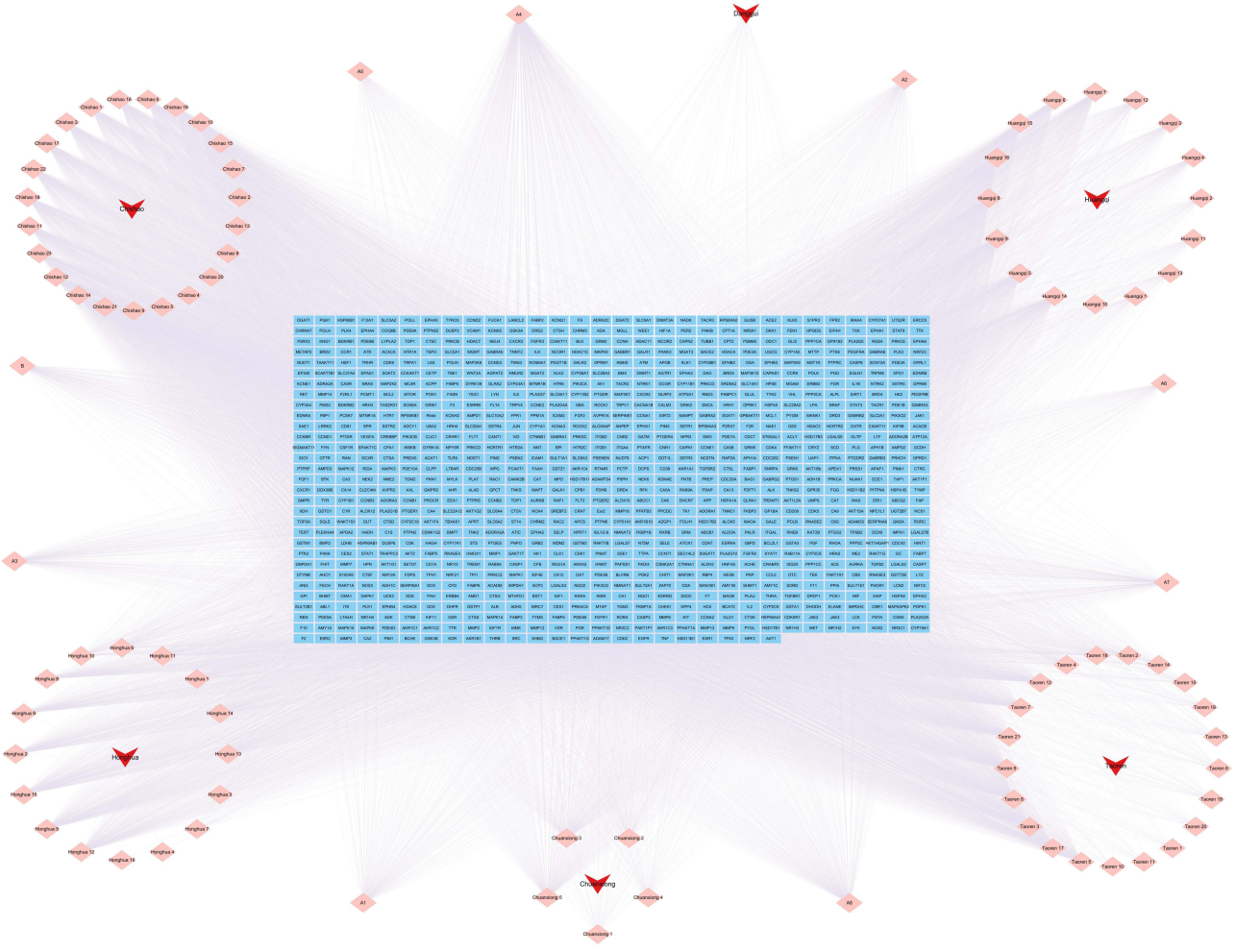

Figure 2 BHD active ingredient-target network.

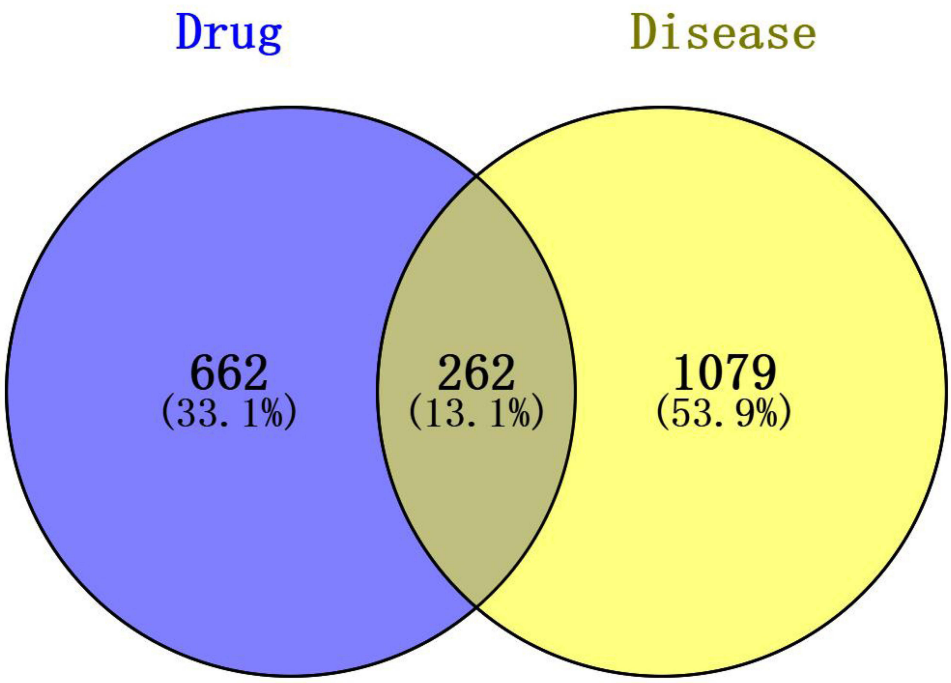

Figure 3 Venn diagram of active ingredients and disease targets.

and TTD databases, and subsequently filtering, integrating, and removing duplicates in Uniprot, a total of 1,341 target genes related to cerebral infarction were collected. Furthermore, the Venn diagram revealed that there are 262 common target genes between BHD and cerebral infarction (Figure 3). The top ten target genes are listed in Table 2.

Core Targets and Pathways of BHD in Cerebral Infarction

The 262 predicted "drug-disease" overlapping genes were entered into the STRING database for protein association analysis. We identified core proteins and used Cytoscape to obtain the PPI network target map for cerebral infarction and BHD. Here, we detail the three nodes with the highest degrees: AKT1, NRF2, and ALB (Figure 4). GO enrichment analysis was conducted using the DAVID database. The results indicated that BHD's effects on cerebral infarction are closely related to various functions, including the negative regulation of phosphorylation, apoptosis processes, positive modulation of cell migration, response to hypoxia, and positive regulation of the phosphoinositide 3-kinase/protein kinase B signaling pathway (Figure 5). KEGG enrichment analysis results suggested that BHD has core target pathways in several signaling pathways related to the treatment of cerebral infarction, including the pathways in cancer, PI3K-Akt

Table 2 Hub Genes Obtained by Topological Analysis

No.	Gene	Degree	Betweenness	Closeness
1	AKT1	354	2989.1953	0.7521614
2	NRF2	344	2323.0706	0.74147725
3	ALB	340	3119.2092	0.7393768
4	TNF	328	2245.1367	0.725
5	TP53	310	1736.094	0.703504
6	CTNNB1	302	2050.5525	0.69786096
7	SRC	302	2023.884	0.696
8	IL1B	300	1502.476	0.69786096
9	EGFR	294	1136.1681	0.68503934
10	STAT3	288	698.3384	0.68503934

https://doi.org/10.2147/DDDT.S503424

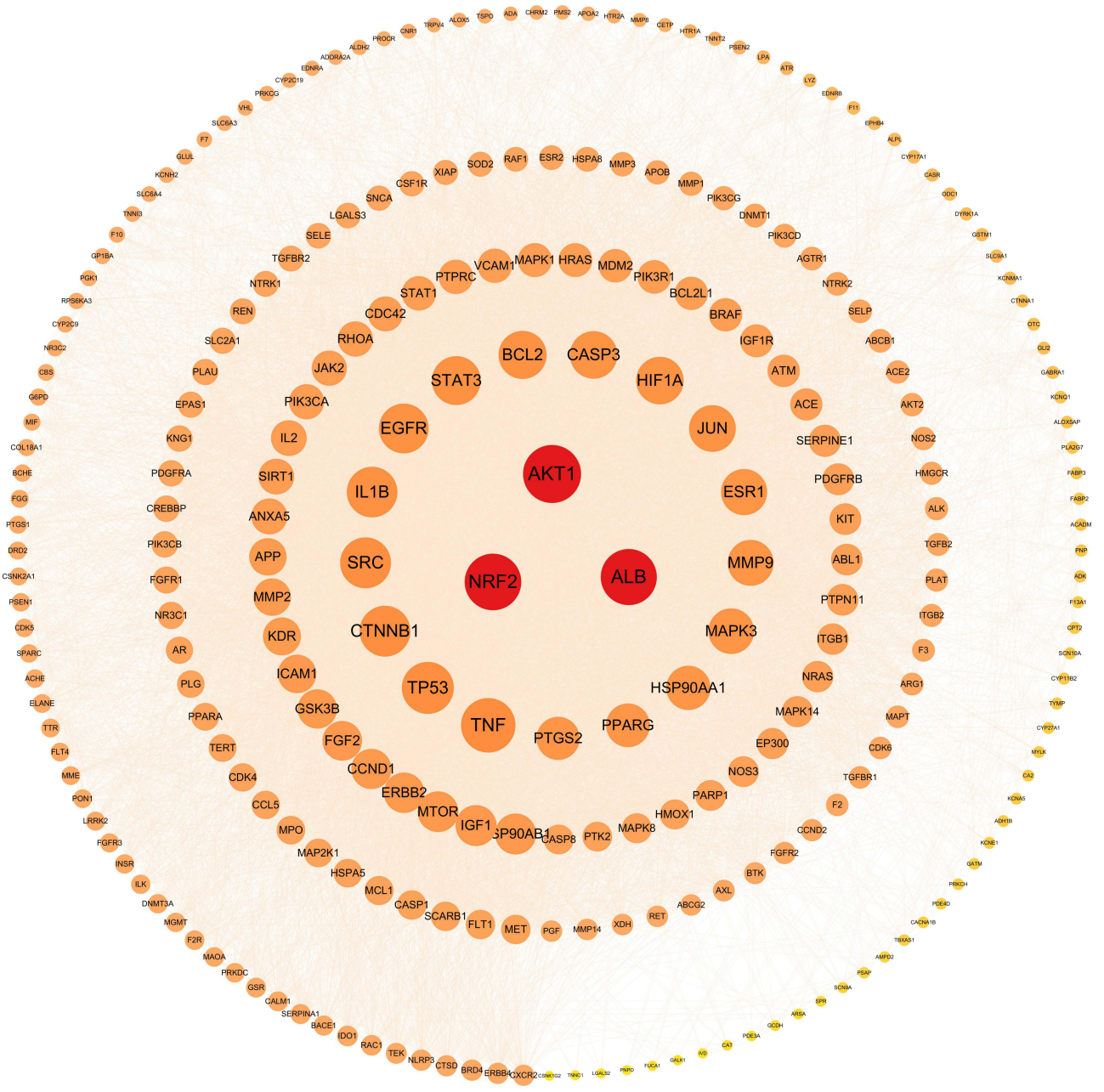

Figure 4 Protein-protein interaction network of common targets of BHD and cerebral infarction.

signaling pathway, MAPK signaling pathway, ferroptosis, and proteoglycans in cancer (Figure 6). Table 3 lists the top 10 pathways. We used Cytoscape 3.7.1 to visualize the top 20 signaling pathways with the smallest P values and their corresponding targets, as shown in the figure (Figure 7).

UPLC-QqQ-MS/MS Quantitative Analysis of Components in BHD

Six components in BHD were identified using the UPLC-QqQ-MS/MS method. The contents of each component are as follows: (1) Calycosin Glucoside: 0.3068 mg/mL,(2) Paeoniflorin: 1.8522 mg/mL,(3) Ferulic Acid: 0.2651 mg/mL,(4) Amygdalin: 0.7799 mg/mL,(5) Hydroxysafflor Yellow A: 0.3206 mg/mL,(6) Kaempferol: 0.0086 mg/mL (Figure 8).

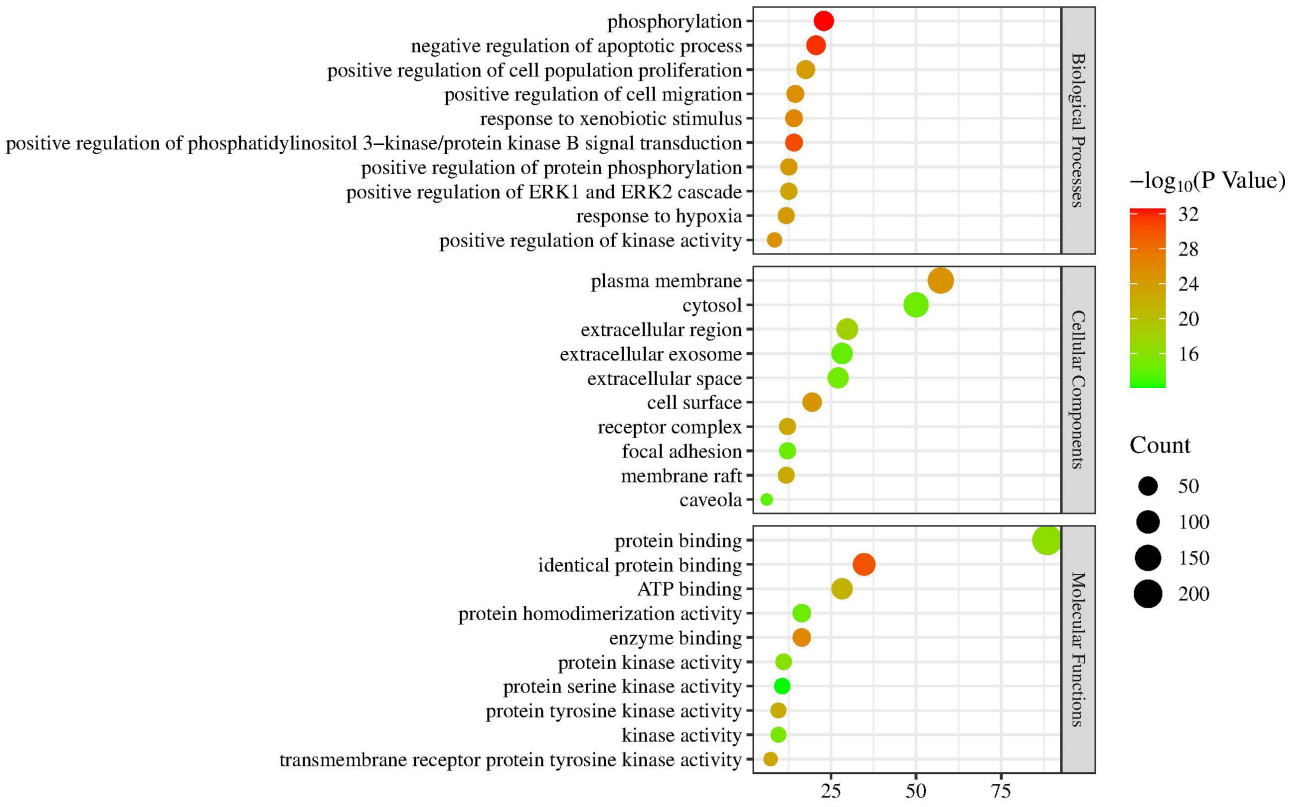

Figure 5 GO functional enrichment analysis.

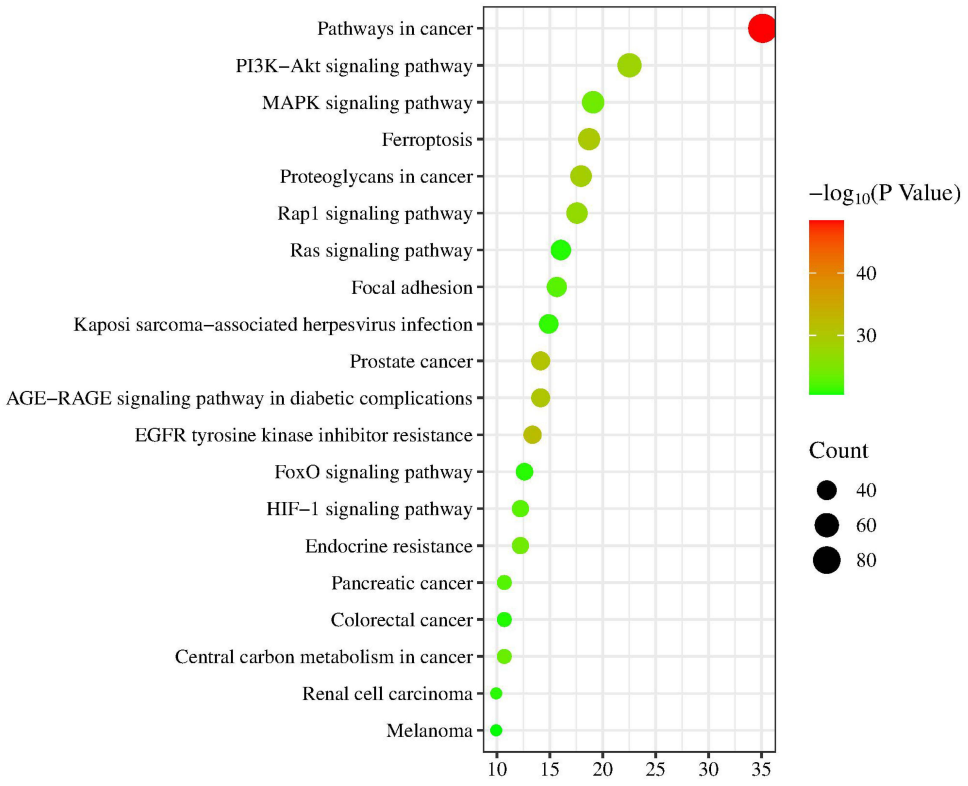

Figure 6 Analysis of KEGG pathway enrichment.

https://doi.org/10.2147/DDDT.S503424

Table 3 Enrichment Analysis of Potential Metabolic Pathways

No.	Pathway Name	Degree
1	Pathways in cancer	92
2	PI3K-Akt signaling pathway	59
3	MAPK signaling pathway	50
4	Ferroptosis	49
5	Proteoglycans in cancer	47
6	Rap1 signaling pathway	46
7	Ras signaling pathway	42
8	Focal adhesion	41
9	Kaposi sarcoma-associated herpesvirus infection	39
10	AGE-RAGE signaling pathway in diabetic complications	37

BHD Improves Neurological Function and Reduces Infarct Size in Ischemic Stroke Mice

Sham and control groups showed no neurological deficits, while the model group had focal impairments. Both high and low doses of BHD significantly improved neurological function compared to the model group (Figure 9A). TTC staining of mouse brain tissue showed similar results. Brain infarcts in the model group appeared distinctly white. The infarct volume in the BHD-treated group was significantly reduced compared to the model group, with a more pronounced reduction observed in the high-dose group (Figure 9B and C). HE staining revealed uniform purple-red staining in brain sections from the sham surgery group, with neurons displaying regular morphology, rich cytoplasm, round nuclei, clear fields of view, and no apparent areas of light staining. In contrast, brain tissue from the ischemic core in the model group exhibited extensive pale staining, accompanied by widespread neuronal liquefactive necrosis and vacuolization. In the BHD-treated group, the area of weak staining in the ischemic core was reduced compared to the model group, although some neurons still showed signs of necrosis (Figure 9D). Nissl staining results were similar. In the hippocampal region of brain tissue from the sham surgery group, neurons were abundant, Nissl bodies appeared deep blue and were evenly distributed, and cell nuclei and nucleoli were transparent, indicating neuronal health with uniform intercellular gaps and no apparent pathological changes. Conversely, neurons in the model group displayed significant structural damage, including nuclear shrinkage, decreased Nissl body counts, and irregular cell structure distribution, indicative of neuronal damage following ischemic brain injury. Neuronal structure in the BHD-treated group was better preserved compared to the model group, with more Nissl bodies and less nuclear shrinkage, suggesting a protective effect of BHD on the mouse model of ischemic stroke (Figure 9E).

BHD Reduces Oxidative Stress and Lipid Peroxidation, Inhibiting Ferroptosis in Ischemic Stroke Mice

We further explored the antioxidative effects of BHD and its role in inhibiting ferroptosis in mice subjected to middle cerebral artery occlusion (MCAO). Compared to the control and sham surgery groups, the model group exhibited significantly elevated MDA levels, indicating increased lipid peroxidation in brain tissues, a hallmark of ferroptosis. BHD treatment significantly reduced MDA levels, suggesting its protective effect against lipid peroxidation (Figure 10A). The activities of key antioxidant enzymes, SOD and GSH, were significantly reduced in the model group, indicating an overwhelmed antioxidant defense system and increased oxidative stress. BHD treatment significantly restored the activities of SOD and GSH, confirming its antioxidative properties (Figure 10B and C). Fe^{2+} levels were significantly elevated in the model group, highlighting its role as a catalyst in lipid peroxidation during ferroptosis. BHD treatment reduced Fe^{2+} levels, especially in the high-dose group, indicating its potential to inhibit ferroptosis by reducing iron levels (Figure 10D).

Transmission electron microscopy (TEM) was used to observe morphological changes in neuronal mitochondria. Neurons from the sham group displayed intact morphology and normal mitochondrial structures. In the model group, severe neuronal damage was observed, characterized by condensed mitochondria, increased mitochondrial membrane density, and reduced

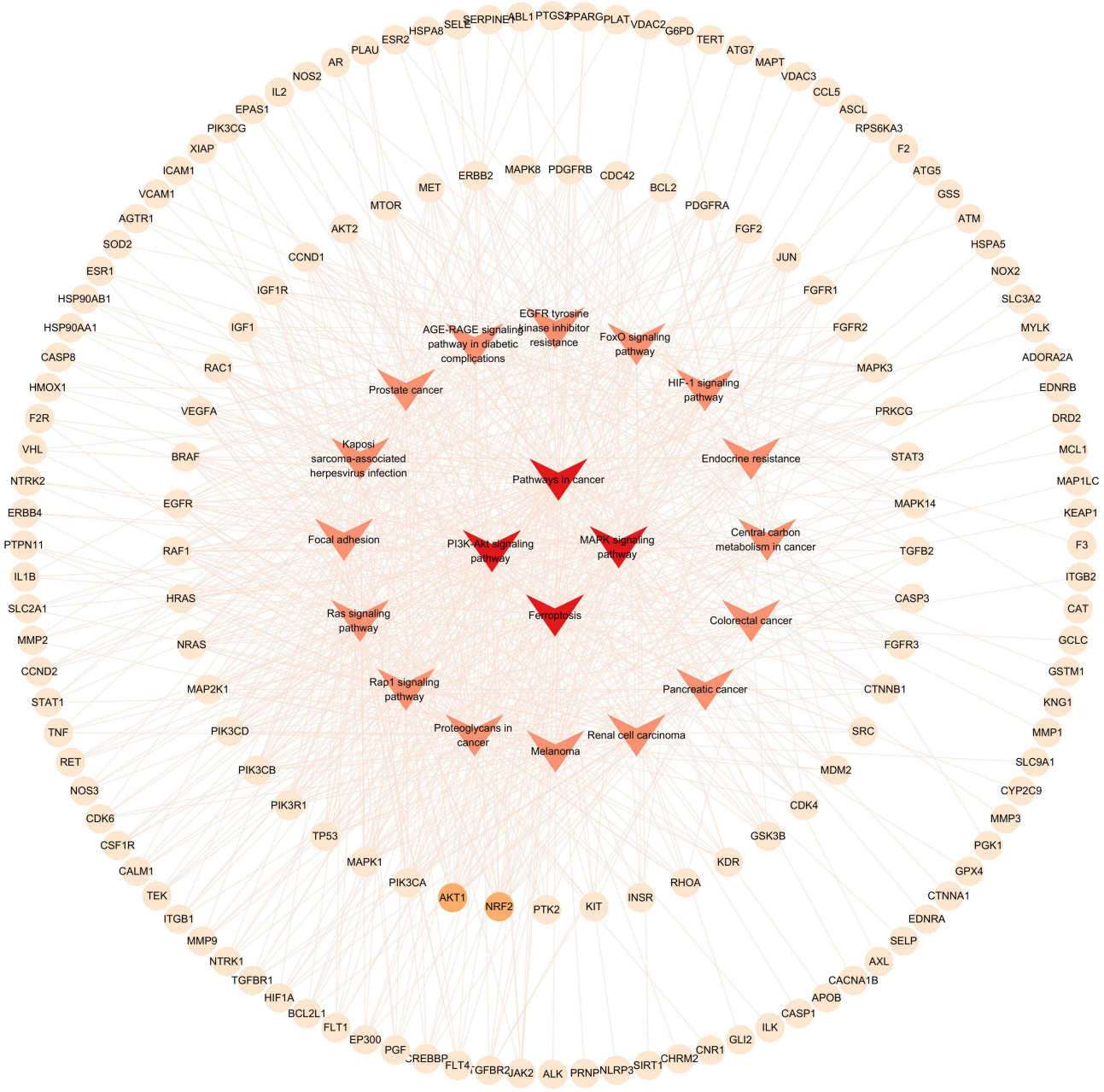

Figure 7 Network of the main pathways and targets of BHD treatment of cerebral infarction.

mitochondrial cristae, consistent with ferroptosis. BHD treatment improved mitochondrial morphology, showing relatively intact cristae and reduced mitochondrial condensation, further supporting its inhibitory effect on neuronal ferroptosis (Figure 10E).

BHD Inhibits Neuronal Ferroptosis by Activating Nrf2 In Vivo

To further investigate the mechanism by which BHD inhibits neuronal ferroptosis, we analyzed the mRNA and protein expression levels of ferroptosis-related proteins in the brain tissues of mice across different groups. The results revealed significant alterations in the levels of these proteins, particularly those associated with the Nrf2 pathway. Compared to the control and sham groups, the mRNA levels of Nrf2, HO-1, and SLC7A11 were significantly reduced in the model group. Specifically, as a key transcription factor for antioxidative stress, the mRNA level of Nrf2 was significantly decreased in the model group, while it was markedly increased in the BHD treatment groups, especially in the high-dose group. HO-1,

https://doi.org/10.2147/DDDT.S503424

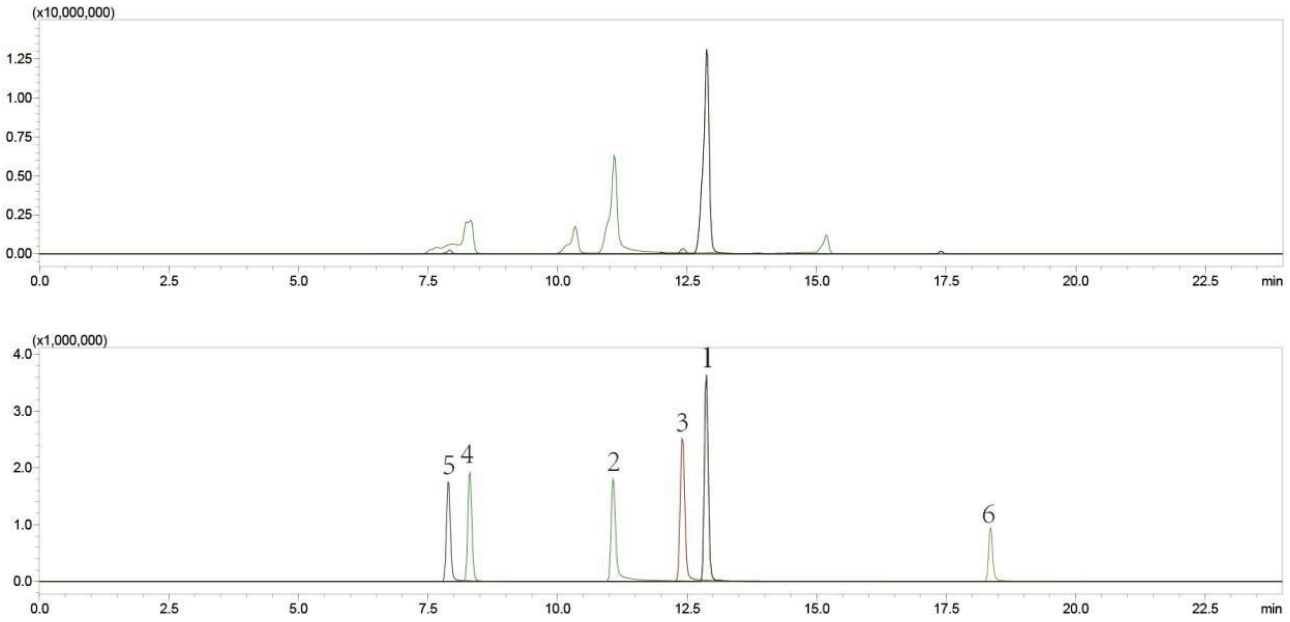

Figure 8 UPLC-QqQ-MS/MS Quantitative Analysis of Components in BHD. 1. Calycosin Glucoside,2. Paeoniflorin,3. Ferulic Acid,4. Amygdalin,5. Hydroxysafflor Yellow A,6. Kaempferol.

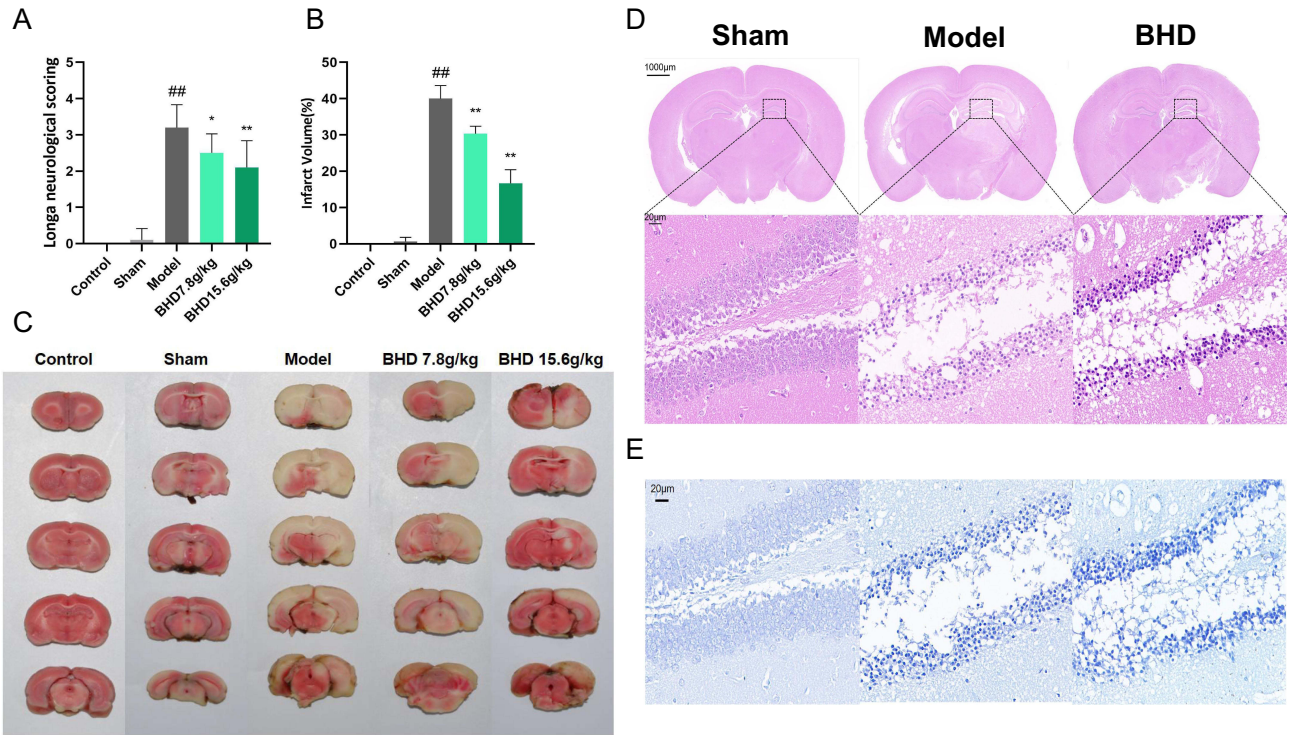

Figure 9 BHD Improves Neurological Function and Reduces Infarct Size in Ischemic Stroke Mice. (**A**) Mice Longa Neurological Function Score. (**B**) Statistical chart of mice brain tissue TTC staining infarct area. (**C**) TTC staining of brain sections. (**D**) HE staining of brain tissue. (**E**) Nissl staining of brain tissue. ##$p < 0.01$: Model vs Sham, *$p < 0.05$, **$p < 0.01$: BHD vs Model, n=6.

a downstream target gene of Nrf2, also showed significantly reduced mRNA levels in the model group, but these levels were significantly restored in both the low-dose and high-dose BHD treatment groups. Additionally, the mRNA levels of SLC7A11 were significantly lowered in the model group and significantly elevated in the BHD treatment groups (Figure 11A–H).

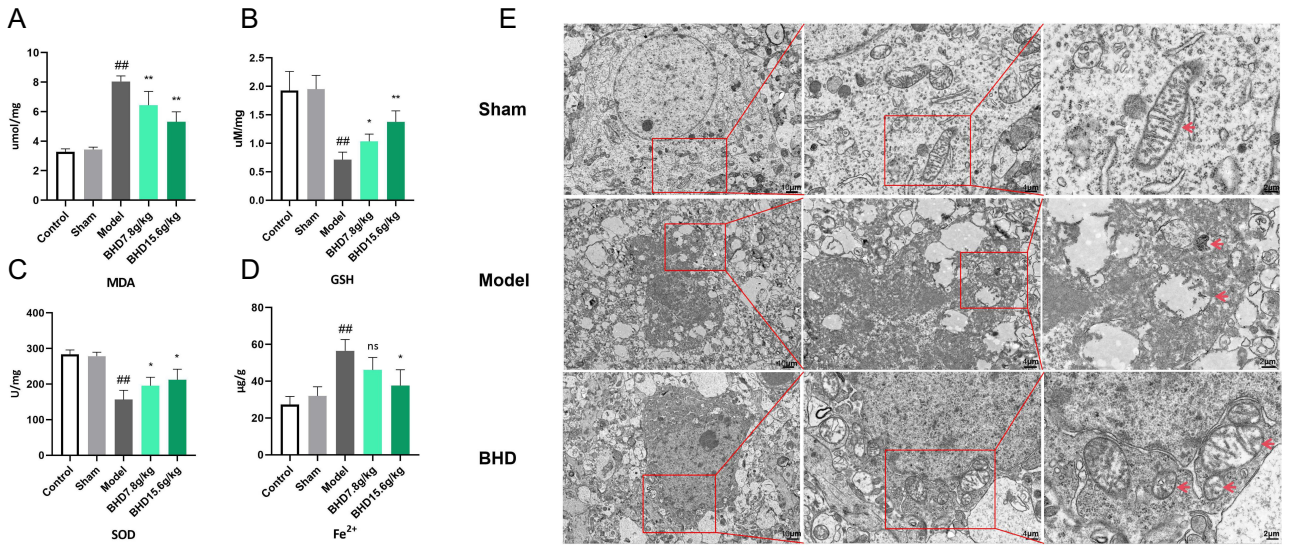

Figure 10 BHD Reduces Oxidative Stress and Lipid Peroxidation, Inhibiting Ferroptosis in Ischemic Stroke Mice. (**A**–**D**) The levels of MDA, GSH, SOD, and Fe^{2+} in the brain tissues of mice from different groups. (**E**) Electron microscopy of mouse brain tissue. Red arrows indicate mitochondria. ##p < 0.01: Model vs Sham, *p < 0.05, **p < 0.01: BHD vs Model, "ns" indicates no significant difference (p > 0.05), n=6.

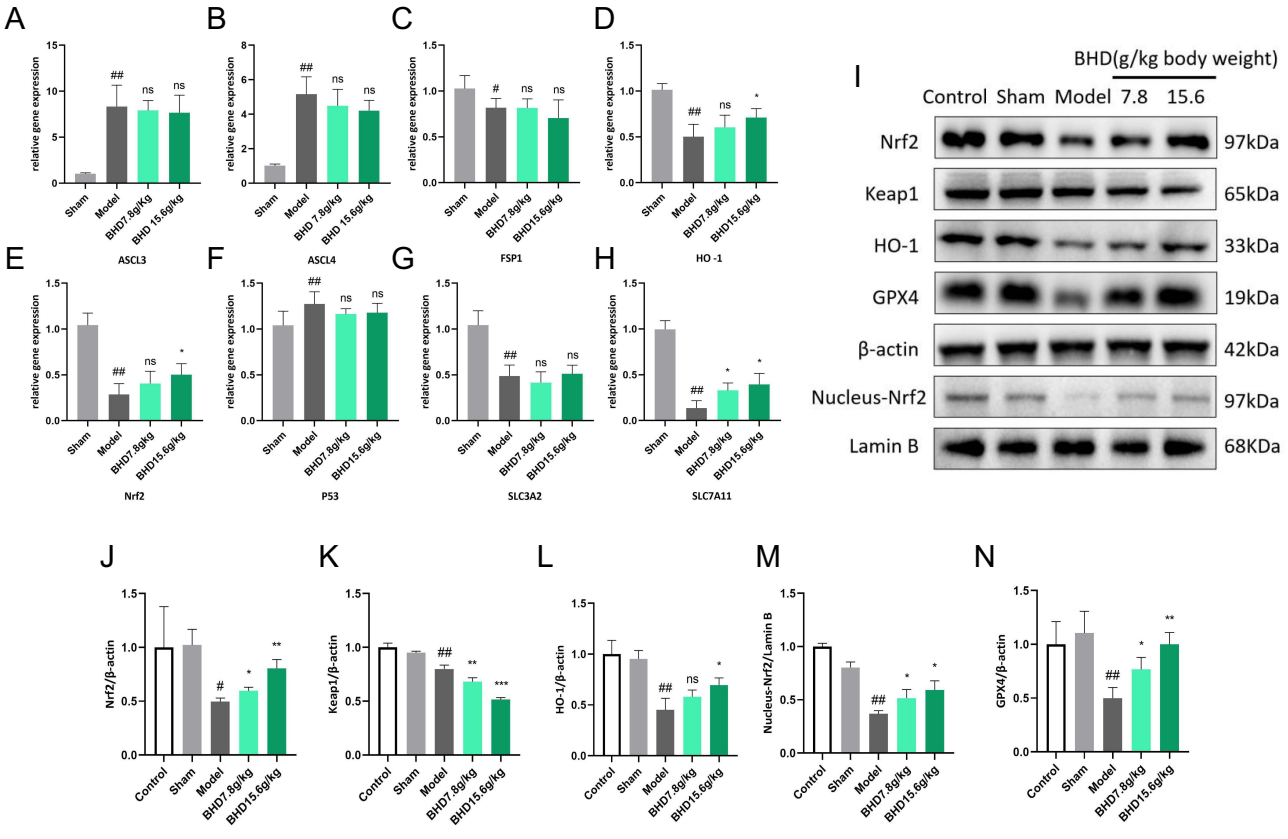

Figure 11 BHD Inhibits Neuronal Ferroptosis by Activating Nrf2 In Vivo. (**A**–**H**) The mRNA levels of SLA3A2, SLA7A11, Nrf2, HO-1, ASCL3, ASCL4, FSP1 and P53 in the brain tissues of mice from different groups. (**I**–**N**) The Western blot results of Nrf2, nucleus Nrf2, Keap1, HO-1 and GPX4 in the brain tissues of mice from different groups. #p < 0.05, ##p < 0.01: Model vs Sham, *p < 0.05, **p < 0.01: BHD vs Model, "ns" indicates no significant difference (p > 0.05), n=6.

https://doi.org/10.2147/DDDT.S503424

To validate these findings at the protein level, we conducted Western blot analysis for Nrf2, GPX4, HO-1, and Keap1. The results showed that, compared to the control and sham groups, the protein levels of Nrf2, GPX4, and HO-1 were significantly reduced in the model group. BHD treatment significantly restored the levels of these proteins, with the high-dose group showing more pronounced effects. However, the level of Keap1 was reduced in the model group and further decreased in the BHD treatment groups. Additionally, the analysis of nuclear Nrf2 levels by Western blot revealed no significant difference between the control and sham groups, whereas the model group exhibited a significant reduction in nuclear Nrf2 levels. Both low-dose and high-dose BHD treatment groups showed an increasing trend in nuclear Nrf2 levels (Figure 11I–N).

BHD Inhibits Neuronal Ferroptosis In Vitro by Reducing Oxidative Stress and Activating Nrf2 Pathway

Using the CCK-8 assay, 2 hours of oxygen-glucose deprivation (OGD) was determined as optimal for inducing significant cell damage while maintaining measurable viability in subsequent experiments (Figure 12A). The results showed that BHD-containing serum significantly increased cell viability in both low-dose and high-dose groups compared to the model group, indicating its protective effect against OGD-induced cell damage (Figure 12B).

Flow cytometry was used to assess reactive oxygen species (ROS) levels in different groups. The model group exhibited a substantial increase in ROS levels, reflecting elevated oxidative stress. In contrast, BHD-containing serum treatment led to a significant reduction in ROS levels. Both low-dose and high-dose BHD-containing serum groups showed markedly lower ROS levels compared to the model group, with the high-dose group displaying the most pronounced reduction. These findings underscore the antioxidative properties of BHD, indicating its capacity to effectively mitigate oxidative stress in HT22 cells (Figure 12C and D).

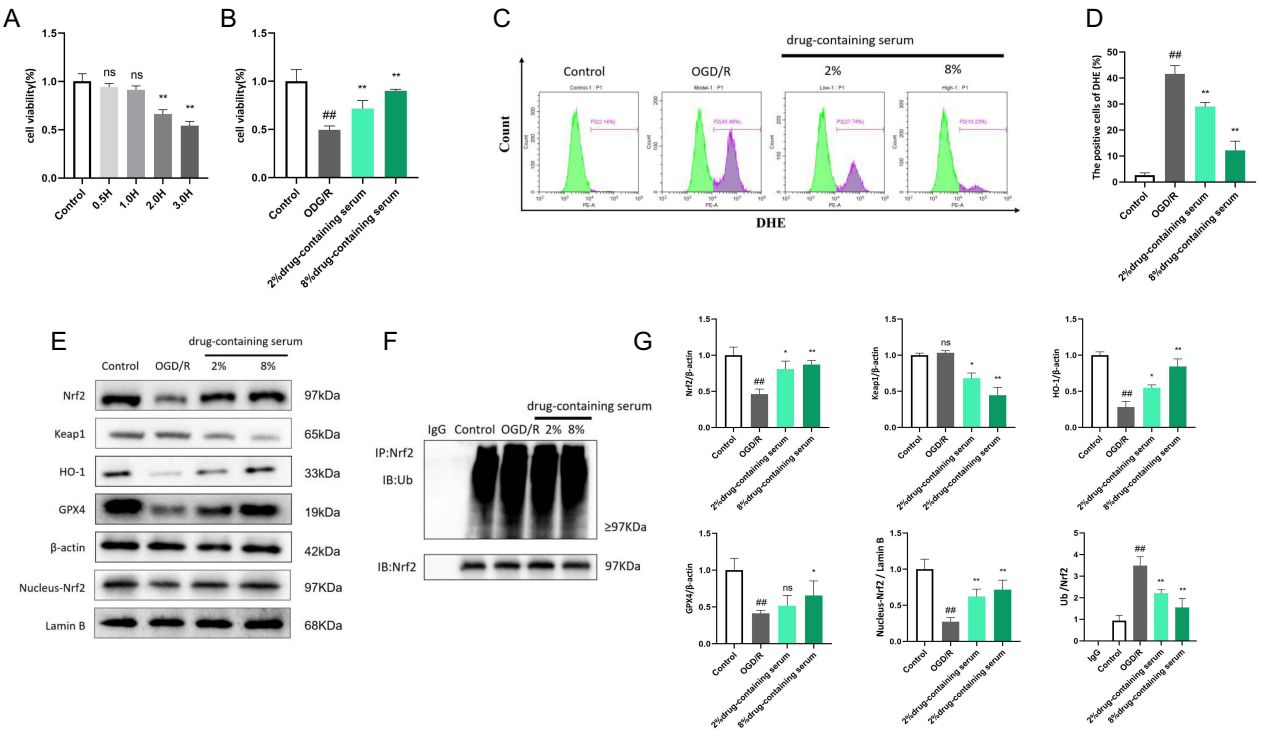

Figure 12 BHD Inhibits Neuronal Ferroptosis in HT22 Cells by Reducing Oxidative Stress and Activating the Nrf2 Pathway. (**A**) CCK-8 assay results showing cell viability in HT22 cells after exposure to varying durations of OGD. (**B**) CCK-8 assay results showing cell viability in different groups of HT22 cells under the selected experimental conditions. (**C**–**D**) Flow cytometry analysis of reactive oxygen species (ROS) levels in different groups. (**E**) Western blot analysis showing the expression levels of various proteins, nuclear Nrf2 levels. (**F**) Immunoprecipitation (IP) results illustrating the ubiquitination levels of Nrf2. (**G**) Statistical graph of WB and IP experiment results. $^{\#\#}p < 0.01$: OGD/R vs Control, $^{*}p < 0.05$, $^{**}p < 0.01$: Serum vs OGD/R, "ns" indicates no significant difference ($p > 0.05$), n=6.

Western blot analysis showed that the model group had lower GPX4, Nrf2, Keap1, and HO-1 protein levels than the control group. BHD-containing serum, especially at higher doses, upregulated GPX4, Nrf2, and HO-1 while further reducing Keap1, indicating Nrf2 pathway activation. Additionally, both doses of BHD-containing serum increased nuclear Nrf2 levels, suggesting Nrf2 nuclear translocation.Lastly, immunoprecipitation (IP) was performed to examine the ubiquitination status of Nrf2. The IP results showed that the model group had a significantly higher level of ubiquitinated Nrf2 compared to the control group, indicating increased degradation of Nrf2 in the absence of BHD. However, BHD-containing serum treatment in both low-dose and high-dose groups significantly reduced the level of ubiquitinated Nrf2, suggesting that BHD inhibits Nrf2 degradation, thereby enhancing Nrf2 activity (Figure 12E–G).

The Necessity of Nrf2 Activation by BHD for Its Protective Effects Against Neuronal Ferroptosis

To confirm the necessity of Nrf2 activation for the protective effects of BHD, we conducted rescue experiments using ML385, an Nrf2 inhibitor, in HT22 cells. When ML385 was added to the high-dose BHD-containing serum group, cell viability was significantly reduced, indicating that the protective effect of BHD on cell viability is mediated by Nrf2 (Figure 13A). Flow cytometry analysis revealed that the addition of ML385 to the high-dose group significantly increased ROS levels, counteracting the antioxidative effects of BHD and highlighting the role of Nrf2 in this process (Figure 13B and E). Western blot analysis showed that the addition of ML385 to the high-dose group significantly decreased the levels of Nrf2, nuclear Nrf2, HO-1, and GPX4 proteins, and increased Keap1 levels, suggesting that ML385 inhibits the activation of the Nrf2 pathway by BHD (Figure 13C and F–J). Immunofluorescence staining and Western blot analysis indicated that BHD-containing serum treatment significantly increased nuclear Nrf2 levels in both low-dose and high-dose groups compared to the model group. The presence of ML385 in the high-dose group significantly reduced nuclear Nrf2 levels, suggesting that ML385 inhibits the BHD-induced nuclear translocation of Nrf2 (Figure 13D and K).

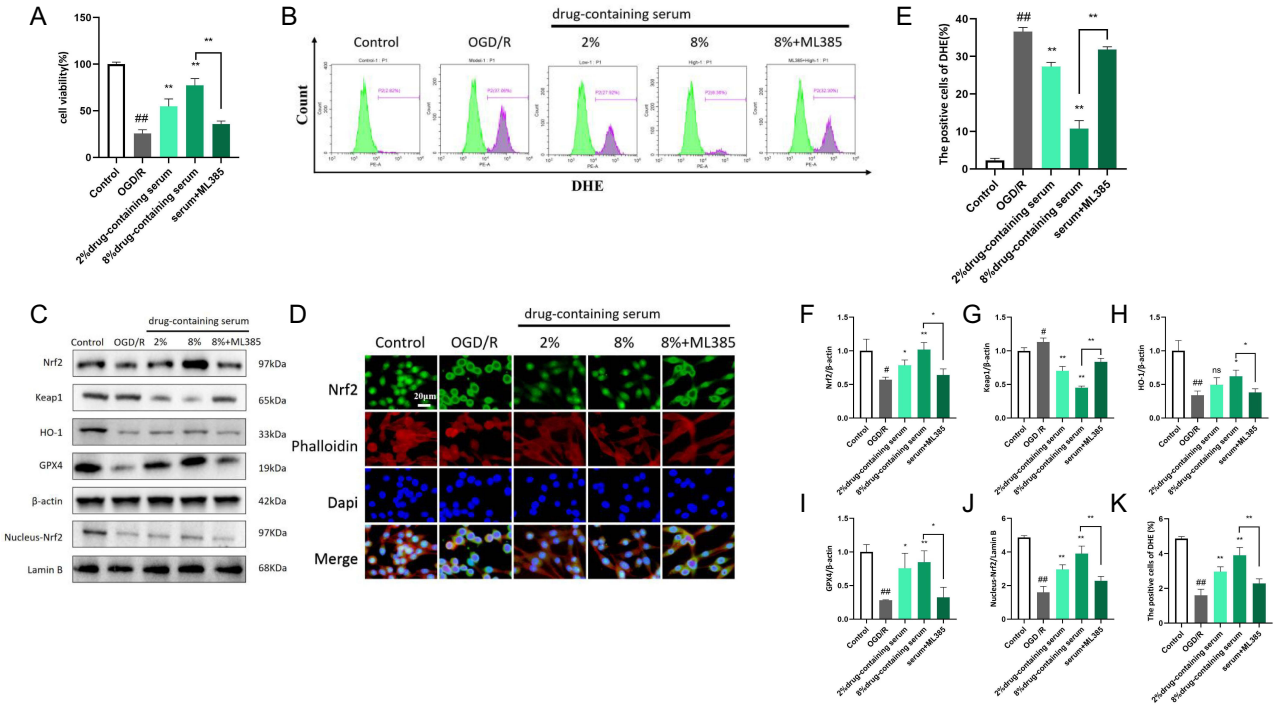

Figure 13 The Necessity of Nrf2 Activation by BHD for Its Protective Effects Against Neuronal Ferroptosis. (**A**) CCK-8 assay results showing cell viability across different groups of neuronal cells. (**B** and **E**) Flow cytometry results showing reactive oxygen species (ROS) levels across different groups. (**C** and **F–J**) Western blot analysis of GPX4, HO-1, Keap1, Nrf2, nuclear Nrf2 levels across groups. (**D** and **K**) Immunofluorescence results showing the nuclear localization of Nrf2 in different groups. $^{\#}p < 0.05$, $^{\#\#}p < 0.01$: OGD/R vs Control, $^{*}p < 0.05$, $^{**}p < 0.01$: Serum vs OGD/R, "ns" indicates no significant difference ($p > 0.05$), n=6.

https://doi.org/10.2147/DDDT.S503424

Discussion

Ischemic stroke is a leading cause of disability and death worldwide, with neuronal injury playing a crucial role in its pathology.[20] Neurons are particularly vulnerable to oxidative stress due to their high levels of polyunsaturated fatty acids and iron, making them susceptible to ferroptosis.[11] One of the critical defense mechanisms against ferroptosis is the reduction of phospholipid hydroperoxides (PL-OOH) to their corresponding phospholipid alcohols (PL-OH) mediated by GPX4.[3,21] However, in both in vitro and in vivo models of ischemia, rapid energy loss leads to impaired function of the glutamate/cystine antiporter System Xc-, resulting in decreased GSH synthesis and a subsequent loss of GPX4's ability to repair lipid peroxides.[22–24] This ultimately leads to a significant amount of neuronal ferroptosis following ischemic stroke.

Ferroptosis is primarily driven by the Fenton reaction, where Fe^{2+} and reactive oxygen species (ROS) serve as powerful oxidants, leading to the peroxidation of phospholipid polyunsaturated fatty acids (PL-PUFA) and initiating cell death.[25] Extensive research has shown that Nrf2 plays a complex role in the metabolism of iron, lipids, and amino acids. Nrf2-knockout animals are notably more susceptible to ischemic stroke,[7,8] emphasizing the importance of this transcription factor in protecting neurons from ferroptosis during ischemic stroke. Nrf2 influences ferroptosis through both antioxidant and non-antioxidant pathways. In the antioxidant pathways, the GSH/GPX4 axis and the FSP1/CoQ10 axis are critical for protecting against ferroptosis. Nrf2 regulates the expression of two key enzymes in GSH biosynthesis,[26] as well as the essential GSH transporter protein SLC7A11 and FSP1.[27,28] Other antioxidant systems, such as peroxiredoxins (PRDX), lower ROS levels, and oxidized PRDX is subsequently reduced by thioredoxin (TXN). Thioredoxin reductase 1 (TXNRD1) utilizes NADPH to reduce oxidized TXN. The expression of PRDX, TXN, and TXNRD1 is regulated at the transcriptional level by Nrf2. In the non-antioxidant pathways, Nrf2 also controls the expression of ferritin, which is responsible for iron ion transport, and FPN1/SLC40A1, which mediates iron efflux from cells.[29,30] Additionally, Nrf2 activation is crucial in reducing the accumulation of PL-PUFA, thereby decreasing the substrates available for ferroptosis.[31] Thus, Nrf2 is a key factor opposing lipid peroxidation and ferroptosis.

This study demonstrates that Buyang Huanwu Decoction (BHD), a traditional Chinese medicine, exerts significant neuroprotective effects in ischemic stroke models by inhibiting ferroptosis through activation of the Nrf2/GPX4 pathway. Network pharmacology provided important insights into BHD's therapeutic effects, revealing multiple pathways associated with cerebral infarction, including ferroptosis, oxidative stress, and PI3K-Akt signaling. Our network pharmacology analysis identified 262 common target genes between BHD and cerebral infarction, highlighting key proteins such as Nrf2, AKT1, and GPX4. The pathway enrichment analysis further demonstrated BHD's ability to modulate critical processes like lipid peroxidation and iron homeostasis, central to ferroptosis inhibition. UPLC-QqQ-MS/MS analysis identified six major chemical components in BHD: Hydroxysafflor Yellow A,[32] Amygdalin,[33] Paeoniflorin,[34] Ferulic Acid,[35] Ononin,[36] and Kaempferol.[37] Each of these compounds is known for its pharmacological properties, including anti-inflammatory, antioxidant, and neuroprotective effects.[38] However, we acknowledge a significant limitation in our current study. We have not explored the synergistic or antagonistic effects among these components. Comprehending how these compounds interact within the formulation is of utmost importance for unlocking BHD's full clinical potential. The combined action of these components could either amplify the therapeutic benefits or lead to unforeseen counter - effects. In future research, we plan to conduct in - depth investigations on the interactions between these compounds. This may involve in vitro and in vivo experiments using various combinations of these components to elucidate their complex relationships.

Our results indicated that BHD notably improved neurological function and lessened infarct size in focal cerebral ischemia mice. We also found that BHD treatment significantly decreased MDA levels and restored antioxidant enzyme activity, suggesting it mitigates oxidative stress and protects neurons from ferroptosis, supporting its potential as a therapeutic agent for oxidative stress - related neuronal damage. These findings are consistent with previous studies reporting the benefits of BHD in stroke recovery.[39] The integration of oxidative stress markers, histological analysis, and mechanistic insights in our study offers a comprehensive view of how BHD impacts stroke pathology. By connecting BHD's traditional use to the modern mechanism of ferroptosis inhibition, our research enhances the scientific credibility of Traditional Chinese Medicine. Clinically, these findings are highly relevant for developing adjunct therapies for ischemic stroke. BHD's potential to tackle oxidative stress and neuronal death can complement existing interventions such as thrombolysis and mechanical thrombectomy. Nevertheless, it's important to note that our findings are pre-clinical, and their applicability to human patients remains

uncertain. Future studies should focus on well - designed clinical trials to validate these pre-clinical results and fully explore BHD's potential in the clinical treatment of ischemic stroke.

Our study demonstrates that BHD effectively activates the Nrf2 pathway, which plays a crucial role in its anti-ferroptotic effects. Specifically, BHD promotes nuclear translocation of Nrf2, leading to activation of downstream antioxidant pathways, such as HO-1 and GPX4 expression. This activation enhances the cell's antioxidant defenses, thereby inhibiting ferroptosis. Additionally, we observed a significant reduction in Keap1 expression in the BHD-treated groups. This finding suggests that BHD may activate Nrf2 by reducing Keap1-mediated ubiquitination, which in turn increases Nrf2's stability and activity. Keap1 is the primary negative regulator of Nrf2, typically promoting Nrf2 ubiquitination and subsequent degradation.As the adaptor protein of the Cullin3-E3 ubiquitin ligase complex, Keap1 interacts with Cul3 and Rbx1 to form a functional E3 ubiquitin ligase (Keap1-Cul3-E3). This complex facilitates the continuous ubiquitination and degradation of Nrf2, ensuring low intracellular levels of Nrf2.[40] This mechanism prevents the excessive activation of downstream antioxidant genes by Nrf2 in the absence of stress signals. However, upon exposure to internal or external stimuli, such as oxidative stress, Keap1 is inactivated due to cysteine residue modifications[41] or competitive binding by p62.[42] This inactivation causes Nrf2 to dissociate from Keap1, preventing newly synthesized Nrf2 from undergoing ubiquitination and degradation by Keap1. By down-regulating Keap1, BHD likely prevents Nrf2 degradation, allowing for Nrf2 accumulation and activation within the nucleus, where it initiates expression of a series of antioxidant genes. In summary, BHD enhances Nrf2 stability and nuclear translocation by reducing Keap1-mediated degradation, thereby activating downstream antioxidant pathways and effectively inhibiting ferroptosis. This mechanism underscores the critical role of the Nrf2 pathway in mediating BHD's protective effects against ferroptosis. However, it should be noted that ferroptosis is a complex process, and other pathways and regulatory factors may also be involved. Future research could explore these potential pathways to further elucidate the mechanism of BHD and potentially identify new therapeutic targets.

This study provides strong evidence that BHD exerts neuroprotective effects in ischemic stroke by inhibiting ferroptosis through activation of the Nrf2/GPX4 pathway. Identification of key chemical components in BHD and confirmation of the necessity of Nrf2 activation for its protective effects pave the way for further research. Future research will consider the long - term neuroprotective effects of BHD, as well as the multi - target effects of multi - drug cooperation. Moreover, the sample size will be further expanded to make the research findings more robust.

Conclusion

In summary, our study shows that Buyang Huanwu Decoction (BHD) provides significant neuroprotection in ischemic stroke models by inhibiting ferroptosis and enhancing neuronal survival. We have preliminarily elucidated the mechanism of BHD, demonstrating that it activates the Nrf2/GPX4 pathway, promotes Nrf2 nuclear translocation, effectively reduces oxidative stress, and inhibits neuronal ferroptosis related to ischemic stroke and reperfusion injury.

Ethics Statement

This research strictly adheres to international and domestic ethical guidelines and legal regulations governing the use of human data. All animal procedures were conducted following the Guidelines for the Ethical Review of Laboratory Animal Welfare (China, 2018) and approved by the Experimental Animal Ethics Committee of Suzhou Hospital of Integrated Traditional Chinese and Western Medicine (Ethics No. 2023009). Additionally, research involving human data was reviewed and approved by the Institutional Review Board (IRB) of Suzhou Hospital of Integrated Traditional Chinese and Western Medicine. Since the study utilized publicly available data with patient informed consent already obtained by the database provider, it was deemed exempt from additional ethical approval under the Measures for Ethical Review of Life Science and Medical Research Involving Human Subjects (China, 2023, Article 32, Items 1 and 2).

Funding

This work was supported by the *Shi Cai School* of Thought Research Special Project (SC2023008), the Wuzhong District Science and Technology Plan Project (WZYW2023016), the Suzhou Science and Technology Bureau under the 2024 Suzhou Applied Basic Research (Medical and Health) Science and Technology Innovation Project (SYWD2024206).

Disclosure

The authors report no conflicts of interest in this work.

References

1. Feigin VL, Stark BA, Johnson CO. Global, regional, and national burden of stroke and its risk factors, 1990-2019: a systematic analysis for the Global Burden of Disease Study 2019. *Lancet Neurol*. 2021;20(10):795–820. doi:10.1016/S1474-4422(21)00252-0
2. Widimsky P, Snyder K, Sulzenko J, Hopkins LN, Stetkarova I. Acute ischaemic stroke: recent advances in reperfusion treatment. *Eur Heart J*. 2023;44(14):1205–1215. doi:10.1093/eurheartj/ehac684
3. Ma T, Du J, Zhang Y, Wang Y, Wang B, Zhang T. GPX4-independent ferroptosis-a new strategy in disease's therapy. *Cell Death Discov*. 2022;8 (1):434. doi:10.1038/s41420-022-01212-0
4. Bu ZQ, Yu HY, Wang J, et al. Emerging Role of Ferroptosis in the Pathogenesis of Ischemic Stroke: a New Therapeutic Target. *ASN Neuro*. 2021;13:17590914211037505. doi:10.1177/17590914211037505
5. Liu C, Wang G, Han W, Tian Q, Li M. Ferroptosis: a potential therapeutic target for stroke. *Neural Regen Res*. 2024;19(5):988–997. doi:10.4103/1673-5374.385284
6. Zhao Y, Liu Y, Xu Y, et al. The Role of Ferroptosis in Blood-Brain Barrier Injury. *Cell mol Neurobiol*. 2023;43(1):223–236. doi:10.1007/s10571-022-01197-5
7. Shih AY, Li P, Murphy TH. A small-molecule-inducible Nrf2-mediated antioxidant response provides effective prophylaxis against cerebral ischemia in vivo. *J Neurosci*. 2005;25(44):10321–10335. doi:10.1523/JNEUROSCI.4014-05.2005
8. Dodson M, Castro-Portuguez R, Zhang DD. NRF2 plays a critical role in mitigating lipid peroxidation and ferroptosis. *Redox Biol*. 2019;23:101107. doi:10.1016/j.redox.2019.101107
9. Hu X, Bao Y, Li M, Zhang W, Chen C. The role of ferroptosis and its mechanism in ischemic stroke. *Exp Neurol*. 2024;372:114630. doi:10.1016/j.expneurol.2023.114630
10. Xu Y, Li K, Zhao Y, Zhou L, Liu Y, Zhao J. Role of Ferroptosis in Stroke. *Cell mol Neurobiol*. 2023;43(1):205–222. doi:10.1007/s10571-022-01196-6
11. Guo J, Tuo QZ, Lei P. Iron, ferroptosis, and ischemic stroke. *J Neurochem*. 2023;165(4):487–520. doi:10.1111/jnc.15807
12. Prass K, Ruscher K, Karsch M, et al. Desferrioxamine induces delayed tolerance against cerebral ischemia in vivo and in vitro. *J Cereb Blood Flow Metab*. 2002;22(5):520–525. doi:10.1097/00004647-200205000-00003
13. Jiang X, Stockwell BR, Conrad M. Ferroptosis: mechanisms, biology and role in disease. *Nat Rev mol Cell Biol*. 2021;22(4):266–282. doi:10.1038/s41580-020-00324-8
14. Gao L, Xiao Z, Jia C, Wang W. Effect of Buyang Huanwu decoction for the rehabilitation of ischemic stroke patients: a meta-analysis of randomized controlled trials. *Health Qual Life Outcomes*. 2021;19(1):79. doi:10.1186/s12955-021-01728-6
15. Wang R, Ren J, Li S, et al. Efficacy evaluation of Buyang Huanwu Decoction in the treatment of ischemic stroke in the recovery period: a systematic review of randomized controlled trials. *Front Pharmacol*. 2022;13:975816. doi:10.3389/fphar.2022.975816
16. Chen X, Chen H, He Y, et al. Proteomics-Guided Study on Buyang Huanwu Decoction for Its Neuroprotective and Neurogenic Mechanisms for Transient Ischemic Stroke: involvements of EGFR/PI3K/Akt/Bad/14-3-3 and Jak2/Stat3/Cyclin D1 Signaling Cascades. *mol Neurobiol*. 2020;57 (10):4305–4321. doi:10.1007/s12035-020-02016-y
17. Yan X, Miao J, Zhang B, et al. Study on semi-bionic extraction of Astragalus polysaccharide and its anti-aging activity in vivo. *Front Nutr*. 2023;10:1201919. doi:10.3389/fnut.2023.1201919.
18. Longa EZ, Weinstein PR, Carlson S, Cummins R. Reversible middle cerebral artery occlusion without craniectomy in rats. *Stroke*. 1989;20 (1):84–91. doi:10.1161/01.str.20.1.84
19. Belayev L, Alonso OF, Busto R, Zhao W, Ginsberg MD. Middle cerebral artery occlusion in the rat by intraluminal suture. Neurological and pathological evaluation of an improved model. *Stroke*. 1996;27(9):1616–1622. doi:10.1161/01.str.27.9.1616
20. Tuo QZ, Zhang ST, Lei P. Mechanisms of neuronal cell death in ischemic stroke and their therapeutic implications. *Med Res Rev*. 2022;42 (1):259–305. doi:10.1002/med.21817
21. Seibt TM, Proneth B, Conrad M. Role of GPX4 in ferroptosis and its pharmacological implication. *Free Radic Biol Med*. 2019;133:144–152. doi:10.1016/j.freeradbiomed.2018.09.014
22. Tuo QZ, Masaldan S, Southon A, et al. Characterization of Selenium Compounds for Anti-ferroptotic Activity in Neuronal Cells and After Cerebral Ischemia-Reperfusion Injury. *Neurotherapeutics*. 2021;18(4):2682–2691. doi:10.1007/s13311-021-01111-9
23. Lan B, Ge JW, Cheng SW, et al. Extract of Naotaifang, a compound Chinese herbal medicine, protects neuron ferroptosis induced by acute cerebral ischemia in rats. *J Integr Med*. 2020;18(4):344–350. doi:10.1016/j.joim.2020.01.008
24. Guan X, Li X, Yang X, et al. The neuroprotective effects of carvacrol on ischemia/reperfusion-induced hippocampal neuronal impairment by ferroptosis mitigation. *Life Sci*. 2019;235:116795. doi:10.1016/j.lfs.2019.116795
25. Dixon SJ, Lemberg KM, Lamprecht MR, et al. Feroptosis: an iron-dependent form of nonapoptotic cell death. *Cell*. 2012;149(5):1060–1072. doi:10.1016/j.cell.2012.03.042
26. Lu SC. Glutathione synthesis. *Biochim Biophys Acta*. 2013;1830(5):3143–3153. doi:10.1016/j.bbagen.2012.09.008
27. Doll S, Freitas FP, Shah R, et al. FSP1 is a glutathione-independent ferroptosis suppressor. *Nature*. 2019;575(7784):693–698. doi:10.1038/s41586-019-1707-0
28. Bersuker K, Hendricks JM, Li Z, et al. The CoQ oxidoreductase FSP1 acts parallel to GPX4 to inhibit ferroptosis. *Nature*. 2019;575 (7784):688–692. doi:10.1038/s41586-019-1705-2
29. Cuadrado A, Rojo AI, Wells G, et al. Therapeutic targeting of the NRF2 and KEAP1 partnership in chronic diseases. *Nat Rev Drug Discov*. 2019;18 (4):295–317. doi:10.1038/s41573-018-0008-x
30. Agyeman AS, Chaerkady R, Shaw PG, et al. Transcriptomic and proteomic profiling of KEAP1 disrupted and sulforaphane-treated human breast epithelial cells reveals common expression profiles. *Breast Cancer Res Treat*. 2012;132(1):175–187. doi:10.1007/s10549-011-1536-9

31. Cho HY, Gladwell W, Wang X, et al. Nrf2-regulated PPARγ expression is critical to protection against acute lung injury in mice. *Am J Respir Crit Care Med*. 2010;182(2):170–182. doi:10.1164/rccm.200907-1047OC
32. Chen G, Li C, Zhang L, et al. Hydroxysafflor yellow A and anhydrosafflor yellow B alleviate ferroptosis and parthanatos in PC12 cells injured by OGD/R. *Free Radic Biol Med*. 2022;179:1–10. doi:10.1016/j.freeradbiomed.2021.12.262
33. Barakat H, Aljutaily T, Almujaydil MS, et al. Amygdalin: a Review on Its Characteristics, Antioxidant Potential, Gastrointestinal Microbiota Intervention, Anticancer Therapeutic and Mechanisms, Toxicity, and Encapsulation. *Biomolecules*. 2022;12(10):1514. doi:10.3390/biom12101514
34. Ren S, Wang Y, Zhang Y, et al. Paeoniflorin alleviates AngII-induced cardiac hypertrophy in H9c2 cells by regulating oxidative stress and Nrf2 signaling pathway. *Biomed Pharmacother*. 2023;165:115253. doi:10.1016/j.biopha.2023.115253
35. Zhang D, Jing B, Chen ZN, et al. Ferulic acid alleviates sciatica by inhibiting neuroinflammation and promoting nerve repair via the TLR4/NF-κB pathway. *CNS Neurosci Ther*. 2023;29(4):1000–1011. doi:10.1111/cns.14060
36. Yu T, Lu X, Liang Y, Yang L, Yin Y, Chen H. Ononin alleviates DSS-induced colitis through inhibiting NLRP3 inflammasome via triggering mitophagy. *Immun Inflamm Dis*. 2023;11(2):e776. doi:10.1002/iid3.776
37. Yuan Y, Zhai Y, Chen J, Xu X, Wang H. Kaempferol Ameliorates Oxygen-Glucose Deprivation/Reoxygenation-Induced Neuronal Ferroptosis by Activating Nrf2/SLC7A11/GPX4 Axis. *Biomolecules*. 2021;11(7):923. doi:10.3390/biom11070923
38. Zhu T, Wang L, Wang LP, Wan Q. Therapeutic targets of neuroprotection and neurorestoration in ischemic stroke: applications for natural compounds from medicinal herbs. *Biomed Pharmacother*. 2022;148:112719. doi:10.1016/j.biopha.2022.112719
39. Shao L, She Y, Yong S, et al. An evidence-based evaluation of Buyang Huanwu decoction for the treatment of the sequelae of stroke: a PRISMA-compliant systematic review and meta-analysis of randomized controlled trials. *Phytomedicine*. 2022;104:154312. doi:10.1016/j.phymed.2022.154312
40. Adinolfi S, Patinen T, Jawahar Deen A, et al. The KEAP1-NRF2 pathway: targets for therapy and role in cancer. *Redox Biol*. 2023;63:102726. doi:10.1016/S1474-4422(21)00252-0
41. Shin JW, Chun KS, Kim DH, et al. Curcumin induces stabilization of Nrf2 protein through Keap1 cysteine modification. *Biochem Pharmacol*. 2020;173:113820. doi:10.1016/j.bcp.2020.113820
42. Komatsu M, Kurokawa H, Waguri S, et al. The selective autophagy substrate p62 activates the stress responsive transcription factor Nrf2 through inactivation of Keap1. *Nat Cell Biol*. 2010;12(3):213–223. doi:10.1038/ncb2021